Surface Roughness Characterization through the Use of Diffuse Component of Scattered Air-Coupled Ultrasound

Japanese Journal of Applied Physics
Vol. 45, No. 5B, 2006, pp. 4534–4540

Surface Roughness Characterization through the Use of Diffuse Component of Scattered Air-Coupled Ultrasound

Deden Dian SUKMANA and Ikuo IHARA

Department of Mechanical Engineering, Nagaoka University of Technology, Kamitomioka 1603-1, Nagaoka, Niigata 940-2188, Japan

(Received November 30, 2005; accepted February 12, 2006; published online May 25, 2006)

Surface roughness characterization through the use of diffuse component of scattered air-coupled ultrasound is presented in this paper. Ultrasonic measurements using broadband air-coupled capacitance transducers with a center frequency of 0.5 MHz have been performed on several specimens with different rms roughness Rq and surface correlation length λ_0 from 0.04 to 244.1 μm and from 29 to 445 μm, respectively. The diffuse components of the scattered ultrasonic waves from the specimens were measured at various scattering angles. It has been shown that the amplitude of diffuse component significantly changes with both the roughness Rq and the surface correlation length λ_0 of the specimen. In order to examine the behavior of the amplitude, the measured results were compared with theoretical ones calculated from a Kirchhoff-based scattering model.
[DOI: 10.1143/JJAP.45.4534]

KEYWORDS: air-coupled ultrasound, surface roughness, surface correlation length, diffuse component, noncontact measurement

1. Introduction

Since the surface roughness of material is closely related to not only optical characteristics of the material surface but also tribological characteristics which affect the mechanical properties of the material and its reliability,[1–3] it is important to evaluate the surface roughness quantitatively. Although two methods, stylus profiling and optical scattering, are well accepted as good conventional methods for measuring surface roughness,[4–9] both of them are not always good enough for practical use in industry, as mentioned in the previous paper.[10] In short, the stylus profiling method has some disadvantages caused by its mechanical contact measurement and the optical scattering method has an upper limit of measurable range of roughness because of the short wavelength of light. Therefore, it would be beneficial to have a technique to realize the quantitative noncontact evaluation of surface topography as well as surface roughness.

It has been considered that ultrasound could be an alternative method for surface roughness evaluation since the roughness evaluation had been performed by electromagnetic waves as well as acoustic waves for many decades.[11] Although some experimental attempts on ultrasonic roughness evaluation have been made,[12–19] most of them have employed immersion techniques which are carried out using water or any liquid as a coupling medium. In many practical cases, however, the use of water or any liquid is often undesirable since they may cause severe degradation of material surfaces having low water resistance. Therefore, the noncontact measurement is much preferable for many industrial applications. To meet such requirements, an air-coupled ultrasound could be a promising candidate because it provides noncontact, nonintrusive measurements without any liquid couplant.[20,21] Although some works on measurement techniques using air-coupled ultrasound have been done,[22–26] the application to surface roughness evaluation has not been found. In our previous paper,[10] we have applied an air-coupled ultrasound with broadband capacitance transducers[21] to the evaluation of surface roughness and have shown the feasibility of air-coupled ultrasonic technique for characterizing rms roughness Rq up to 244.1 μm: the scattered waves from material surfaces were measured and it was then shown that the Rq which mainly reflects height information of surface geometry can be characterized from the coherent component of the scattered waves. However, it seems to be difficult to characterize lateral information of the surface geometry from only the coherent component. Such lateral information is also important to obtain more detailed description of the surface geometry. In the present paper, the diffuse component of the scattered wave is used for characterizing both the Rq and the surface correlation length λ_0 which relates to the lateral information of the surface geometry. A pair of broadband capacitance transducers has been used in a reflection configuration to measure the diffuse components of scattered waves from rough surfaces. The relationships between the amplitude of the diffuse component and two kinds of surface roughness parameters, the Rq and λ_0 have been examined. The Kirchhoff-based scattering model[27] has been used to verify the validity of the experimental results.

2. Scattered Ultrasonic Waves from Rough Surfaces

Figure 1 shows a schematic view of the energy distribution of the scattered waves when a plane ultrasonic wave is incident to material surface having random roughness.[28] For a smooth surface, there exists mainly a specular reflection with an angle symmetric to the incident angle, as shown in Fig. 1(a). As the surface roughness increases, a specular reflection and diffuse reflection exists, as shown in Fig. 1(b). The specular reflection is called the coherent component, while the diffuse reflection is called the diffuse component. Rougher surface increases the diffuse component and reduces the coherent component, as shown in Fig. 1(c). Although there are many theoretical studies on ultrasonic wave scattering from rough surfaces,[29–34] the Kirchhoff theory is widely used for investigating the scattering phenomena because of its comprehensible physical basis and relatively simple analytical expression for the scattered ultrasonic field. Using the Kirchhoff theory under some assumptions, such as plane wave incidence, a single scattering event, Gaussian distribution of surface height, Gaussian correlation function of surface height, and far field conditions, the scattered field can be considered to be a

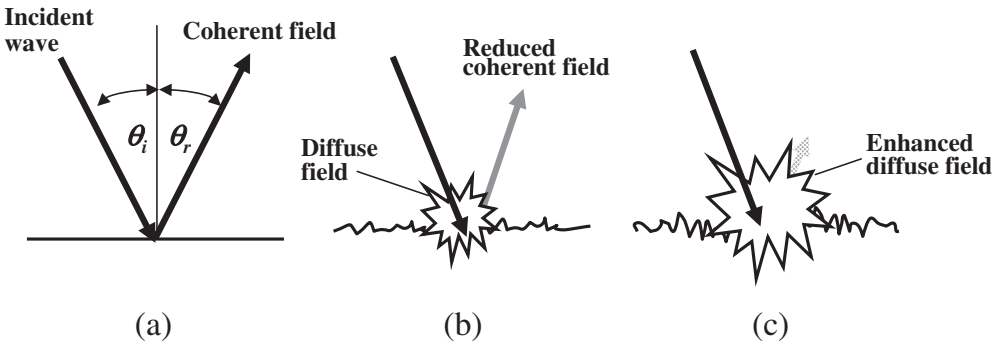

Fig. 1. Schematic view of the change in scattered energy distribution as roughness increases: (a) smooth surface (b) slightly rough surface (c) rough surface.

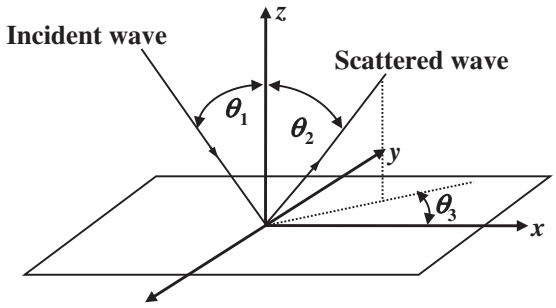

Fig. 2. Scattering geometry used in the experiment.

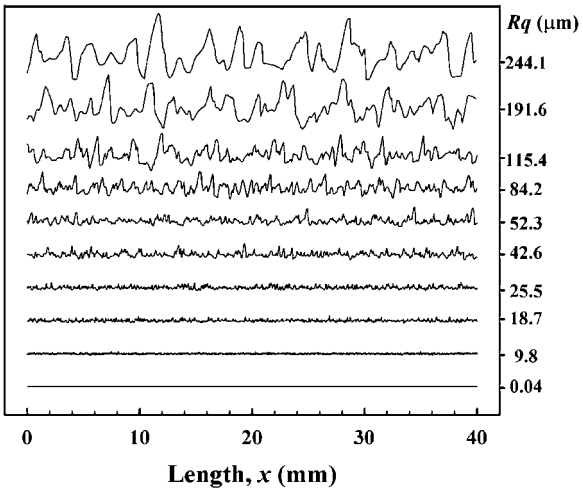

Fig. 3. Surface profiles of the specimens measured by a stylus method.

superposition of coherent and diffuse components. The intensity of the overall scattered field can then be written as[27]

$$I = I_{\text{coherent}} + I_{\text{diffuse}}. \tag{1}$$

The coherent component of the scattered field is regular and in phase with the incident wave, while the diffuse component is irregular and has a lack of phase matching with the incident wave. For scattering geometry shown in Fig. 2, the intensity of the diffuse component is given by[27]

$$I_{\text{diffuse}} = \frac{k^2F^2\lambda_0^2 e^{-g}}{4\pi r^2} A_M \sum_{n=1}^{\infty} \frac{g^n}{n!n} \exp\left[-\frac{k^2(A^2+B^2)\lambda_0^2}{4n}\right], \tag{2}$$

where k is the wave number, r is the distance of the scattering point away from the surface, A_M is the insonified surface area, and λ_0 is the surface correlation length. The parameters g, F, A, and B in eq. (2) are defined as

$$g = k^2Rq^2(\cos\theta_1 + \cos\theta_2)^2, \tag{3}$$

$$F = \frac{1 + \cos\theta_1\cos\theta_2 - \sin\theta_1\sin\theta_2\cos\theta_3}{\cos\theta_1 + \cos\theta_2}, \tag{4}$$

$$A = \sin\theta_1 - \sin\theta_2\cos\theta_3, \tag{5}$$

$$B = -\sin\theta_2\sin\theta_3, \tag{6}$$

where Rq is the rms roughness, θ_1 is incident angle and both of θ_2 and θ_3 are scattering angles. We can see from eq. (2) that the scattered ultrasonic field is related to the two surface roughness parameters, Rq and λ_0. Since the coherent component is closely related to only Rq,[10] the two roughness parameters could be quantitatively evaluated from the coherent and diffuse components.

3. Experiment

3.1 Specimens

Nine sheets of sandpaper having different grit sizes are used for the specimens. The sandpapers are bonded to a steel plate to make them flat. A polished stainless-steel plate is used as a reference specimen having a smooth surface. Figure 3 shows the surface profiles of the specimens measured by a stylus profilometer (Tokyo Seimitsu, SURFCOM3000A,) using a 2 μm radius tip with 0.7 mN stylus load traced in a length of 40 mm on the surfaces. The statistical parameters for describing surface roughness of the specimen in this work are rms roughness Rq and surface correlation length λ_0. Rq represents the vertical surface roughness and is essentially calculated as the variance of the vertical dimension of the surface height $h(x)$. In the discrete case, Rq is given by[35]

$$Rq = \sqrt{\frac{1}{N}\sum_{i=1}^{N}[h_i - \bar{h}]^2}, \tag{7}$$

where N is the number of data points, h_i is the height at each point in the surface profile, and $\bar{h}$ is the average height in the surface profile. The Rq of the specimens are in the range from 0.04 to 244.1 μm, as shown in Fig. 3. On the other hand, surface correlation length is used for the horizontal

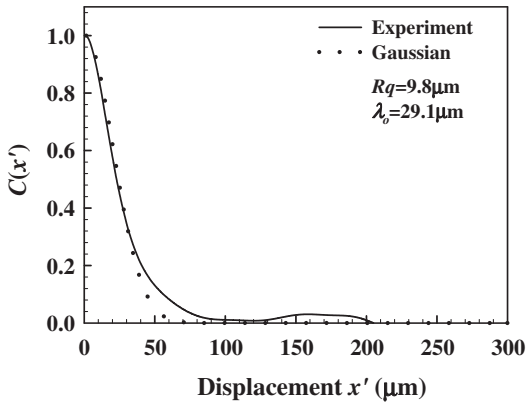

(a)

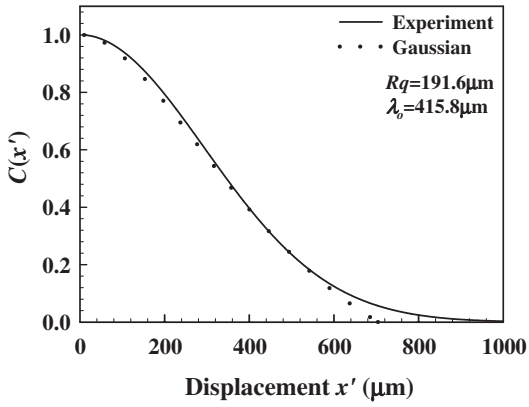

(b)

Fig. 4. Autocorrelation function of the height of the specimens having roughness Rq of 9.8 μm (a) and 191.6 μm (b).

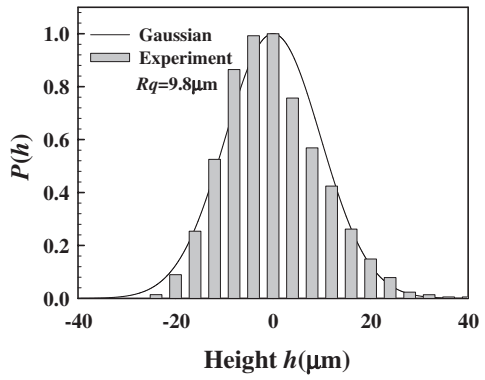

(a)

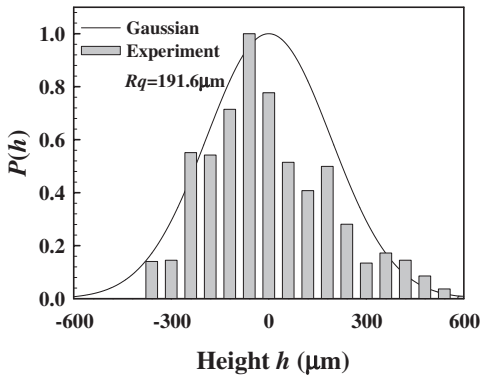

(b)

Fig. 5. Probability density of the height of the specimens having roughness Rq of 9.8 μm (a) and 191.6 μm (b).

description of the surface roughness. The surface correlation length is obtained from autocorrelation function of surface height $h(x)$. The autocorrelation function for a spatial displacement of $x' = n\Delta x$ is given by[35]

$$C_n = \frac{1}{Rq^2(N-n)} \sum_{i=0}^{N-n} (h_i - \bar{h})(h_{i+n} - \bar{h}), \tag{8}$$

where h_{i+n} is a point with a spatial displacement from the point h_i, n is an integer ≥ 0. The surface correlation length λ_0 is defined as the distance x' for which $C(x')$ is equal to $1/e$, that is

$$C(\lambda_0) = 1/e. \tag{9}$$

The surface correlation describes the statistical independence of two points on the surface and the surface correlation length is a distance at which two points can be considered to be uncorrelated each other. The λ_0 of sandpaper sheets used are in the range from 29 to 445 μm. Figure 4 shows the autocorrelation functions of the surface height for two specimens having $Rq = 9.8$ and 191.6 μm. The dotted lines in Fig. 4 are the theoretical Gaussian correlation functions calculated from the same λ_0 as the measured one. We can see that the correlation function for each specimen is well approximated by the Gaussian. We also calculate the probability density of the surface height $P(h)$ to verify whether the specimens satisfy the assumption that their surface height distributions are Gaussian or not. Figure 5 shows the probability density of the surface height for two specimens of $Rq = 9.8$ and 191.6 μm. The solid lines in Fig. 5 are the theoretical Gaussian distribution calculated with the variance corresponding to the measured probability density. We can see that for the specimens having small Rq, such as 9.8 μm shown in Fig. 5(a), the height distribution closely matches the Gaussian distribution, while the height distribution deviates slightly from the Gaussian for the specimen having large Rq, such as 191.6 μm shown in Fig. 5(b).

3.2 Experimental setup

The experimental setup used in this work is shown in Fig. 6. The measurement system mainly consists of a pair of broadband air-coupled capacitance transducers (Micro Acoustic, BAT) having a center frequency of 0.5 MHz, a square-wave pulser (Ritec, SP-801A) and a broadband receiver (Ritec, BR-640A) used to transmit and receive wide-band ultrasonic pulse waves, respectively. The diameter of each transducer is 10 mm. The distance between the transducers and specimen surface is about 35 mm. The ultrasonic signals are acquired using a serial acquisition board at a sampling rate of 100 MHz, then signal processing and data analysis are performed with personal computer (PC) running LabView software.

Pulse-echo measurements are taken using the transducers operating with a repetition rate of 0.5 kHz. The ultrasonic waves are incident to the specimen surface with an incident angle of 60° and scattered waves are measured in two different scattering planes, x–z and x–y planes, as shown in Fig. 2. The scattered waves in the x–z plane are measured at

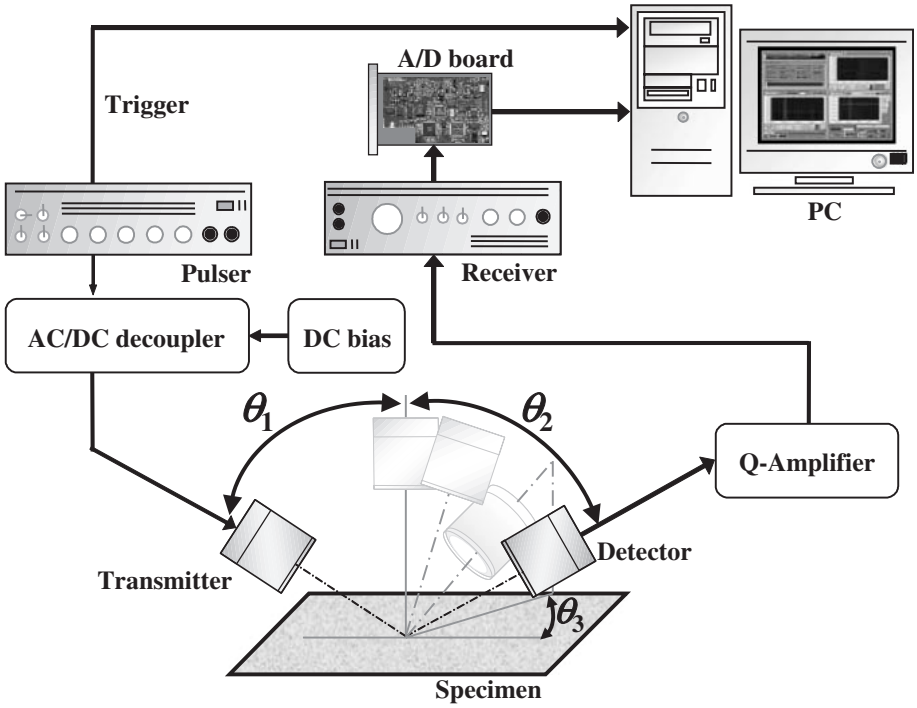

Fig. 6. Surface roughness measurement system using air-coupled ultrasound.

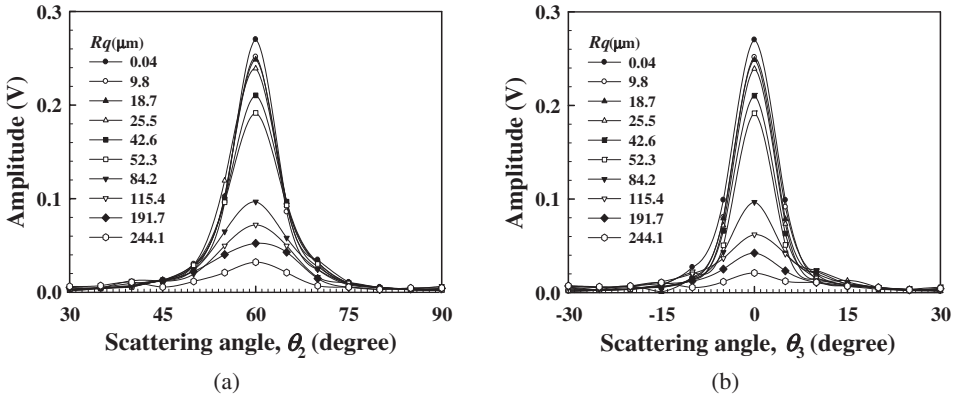

Fig. 7. Change in the amplitudes with the scattering angles for each specimens measured at x–z plane with $\theta_1 = 60^\circ$ and $\theta_3 = 0^\circ$ (a) and x–y plane with $\theta_1 = \theta_2 = 60^\circ$ (b).

various angles of θ_2 from 0 to 90° at interval of 5° under the condition of $\theta_3 = 0^\circ$, while those in the x–y plane are measured at various angles of θ_3 from −70 to 70° under the condition of $\theta_2 = 60^\circ$. In order to reduce the background noise of the measured signals, the average values are obtained from hundred acquired signals at each scattering angle. Five independent measurements are made at different locations for each specimen and the average values of the peak-to-peak amplitude of the measured signal are used for discussion.

4. Results and Discussion

Figure 7(a) shows the change in the amplitude of the scattered waves with the scattering angle θ_2 for each specimen and Fig. 7(b) shows the change with the scattering angle θ_3. We can see that each curve of the amplitude change has a peak at $\theta_2 = 60^\circ$ in Fig. 7(a) and $\theta_3 = 0^\circ$ in Fig. 7(b), respectively. Each angle is the specular reflection angle at which the coherent component is dominant in the reflected wave. The coherent components from the irradiated area are in-phase and therefore such phase matching among the components makes a strong reflection. We can see that the coherent component decreases as Rq increases. This is because the energy of incident ultrasonic wave is partly scattered into various angles reducing the coherent energy reflected in the specular direction as Rq increases. The relationships between such coherent component and surface roughness have been discussed in the previous paper.[10] In this paper, we focus on the relationship between the amplitude of the scattered waves in non-specular reflection angle and surface roughness. It is shown in Fig. 7(a) that the amplitude for each specimen drastically decreases as the scattering angle departs from the specular reflection angle of 60°. For non-specular reflection angles which are more than 20° away from the specular reflection angle, it is considered that there are no more coherent components and only diffuse

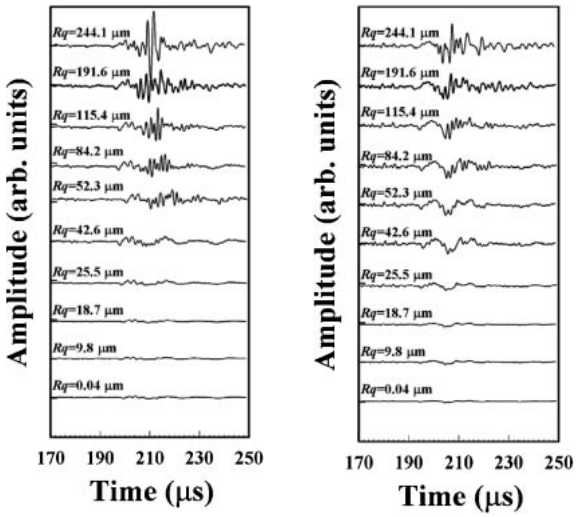

Fig. 8. Change in the waveforms of the diffuse components with the roughness Rq obtained at x–z plane with $\theta_1 = 60^\circ$, $\theta_2 = 30^\circ$ and $\theta_3 = 0^\circ$ (a) and x–y plane with $\theta_1 = \theta_2 = 60^\circ$ and $\theta_3 = 30^\circ$ (b).

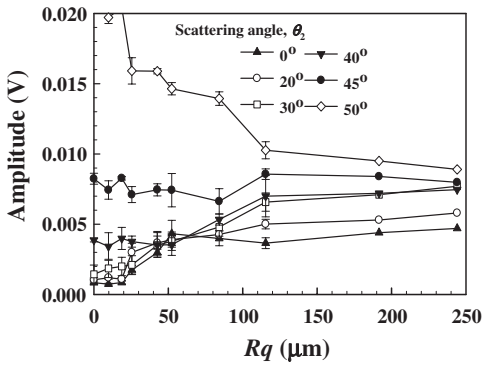

Fig. 9. The relationship between the roughness Rq and the amplitude for various scattering angles of θ_2 obtained at x–z plane with $\theta_1 = 60^\circ$ and $\theta_3 = 0^\circ$.

components exist in the scattered wave. Since the diffuse component is scattered into various directions under the condition of out-of-phase, the amplitude of the component is quite small compared to that of coherent component. Figure 8 shows the waveforms measured at the angles of $\theta_2 = 30^\circ$ and $\theta_3 = 0^\circ$ (a) and at the angles of $\theta_2 = 60^\circ$ and $\theta_3 = 30^\circ$ (b). We can see in both waveforms that the amplitude increases as roughness Rq increases. This tendency is opposite to that of the coherent component.[10] The fact that the waveforms do not remain regular during the amplitude change with Rq reveals that the observed scattered waves are diffuse components. Although the amplitude of the scattered waves in x–y plane is slightly smaller than that in x–z plane as shown in Fig. 8, no significant difference between Figs. 8(a) and 8(b) is observed. This is because the surface topography of the sandpapers used is considered to be isotropic and homogenized without any predominant direction of the surface texture. Figure 9 shows the relationship between the Rq and the amplitude for various angles of θ_2, obtained from Fig. 7(a).

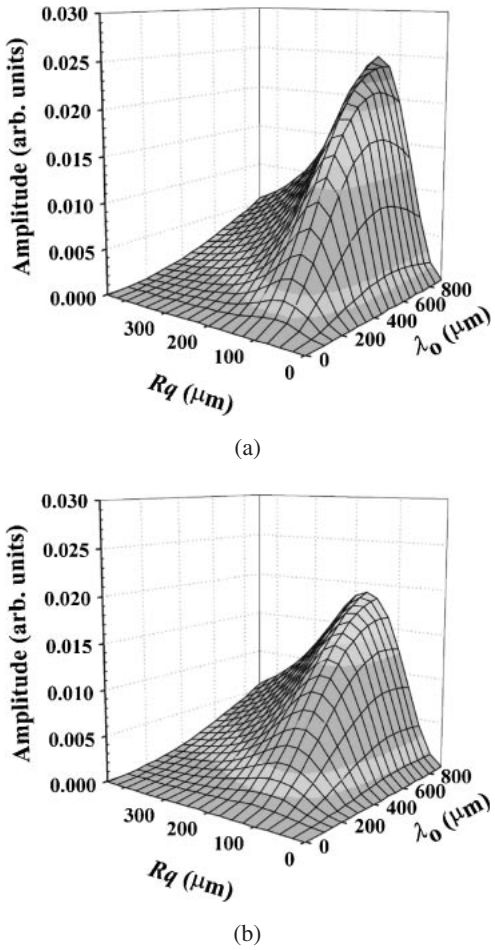

Fig. 10. The amplitude distribution of diffuse component as functions of roughness Rq and surface correlation length λ_0 obtained at x–z plane with $\theta_1 = 60^\circ$, $\theta_2 = 30^\circ$ and $\theta_3 = 0^\circ$ (a) and x–y plane with $\theta_1 = \theta_2 = 60^\circ$ and $\theta_3 = 30^\circ$ (b).

For the angle of 50° which is close to specular reflection angle, the amplitude decreases with Rq. This is similar to the behavior of the coherent component.[10] For the angles up to 40° at which diffuse components are dominant, however, the amplitude increases with Rq. We can also see in Fig. 9 that the amplitude is almost constant for the angle of 45°. It is probable that the angle of 45° is a transition angle from coherent to diffuse. It is noted that the similar behavior to that shown in Fig. 9 is observed for the scattering angles of θ_3 in the x–y plane.

It can be seen from eq. (2) that the amplitude of diffuse component depends not only on Rq but also on surface correlation length λ_0. Understanding of the influence of both of Rq and λ_0 on the amplitude of diffuse component is therefore an important aspect for evaluating surface roughness from the scattered wave. The variations of the amplitude are calculated from eq. (2) as functions of Rq and λ_0 and shown in Fig. 10. Figures 10(a) and 10(b) are for the scattering angles of $\theta_2 = 30^\circ$ and $\theta_3 = 0^\circ$ and for $\theta_2 = 60^\circ$ and $\theta_3 = 30^\circ$, respectively. The other parameters used for the calculation are the same as those used in the experiment mentioned above. We can see that Figs. 10(a) and 10(b) are very similar but the amplitude in x–y plane calculated with $\theta_3 = 30^\circ$ is smaller than that in x–z plane calculated with $\theta_3 = 0^\circ$. Such tendency is also found in the

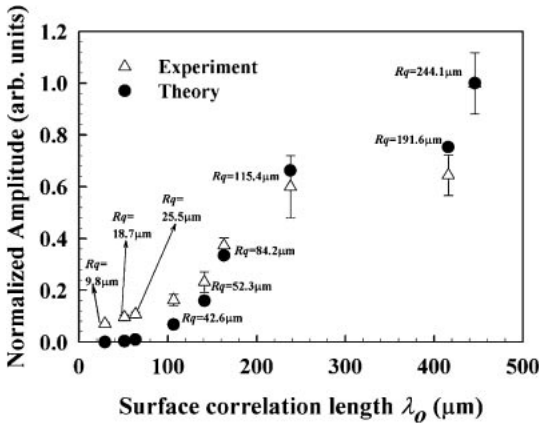

(a)

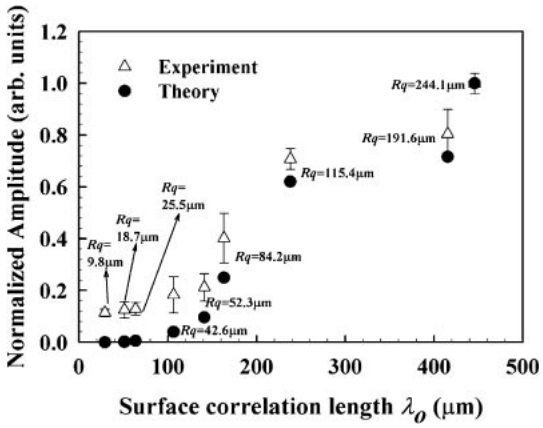

(b)

Fig. 11. The relationship between the surface correlation length λ_0 and the amplitude of the diffuse component obtained at x–z plane with $\theta_1 = 60^\circ$, $\theta_2 = 30^\circ$ and $\theta_3 = 0^\circ$ (a) and x–y plane with $\theta_1 = \theta_2 = 60^\circ$ and $\theta_3 = 30^\circ$ (b).

experimental results shown in Fig. 8. It should be noted that the amplitude of diffuse component is very sensitive to both Rq and λ_0. It can be seen from Fig. 10 that the surface correlation length λ_0 which is somewhat difficult to evaluate quantitatively, may be obtained from the diffuse component when the Rq is known. Figure 11 shows the relationship between the λ_0 and the amplitude of the diffuse component for each specimen, where the amplitude is normalized by dividing by the amplitude of the specimen having $Rq =$ 244.1 μm and the λ_0 is measured using a stylus profilometer. Figures 11(a) and 11(b) are for the scattering angles of $\theta_2 = 30^\circ$ and $\theta_3 = 0^\circ$ and for $\theta_2 = 60^\circ$ and $\theta_3 = 30^\circ$, respectively. The measured relationships between the amplitude and the λ_0 almost agree with the theoretical ones. A discrepancy between the experimental and theoretical results is found for specimens having Rq less than 52.3 μm. This is because the amplitude of the diffuse component is quite small for such small Rq and therefore it is comparable with the inherent noise in measured signals. Such the noise creates the discrepancy between theoretical and experimental results. In order to make sure that the λ_0 can be correctly estimated from the diffuse component, further works such as an experimental demonstration for determining λ_0 using the specimens with identical values of Rq but different values of λ_0, will be made in near future.

5. Conclusion

Air-coupled ultrasound with broadband capacitance transducers having a center frequency of 0.5 MHz has been applied to the evaluation of surface roughness of the specimens having rms roughness Rq and surface correlation length λ_0 in the range from 0.04 to 244.1 μm and from 29 to 445 μm, respectively. The relationships between the surface roughness and the amplitude of the diffuse components of the scattered wave have been obtained and verified using the Kirchhoff-based scattering model. It has been found experimentally that the behaviors of the diffuse component with surface roughness are quite different from those of the coherent component. Since the amplitude of the diffuse component is very sensitive to both Rq and surface correlation length λ_0, it could be possible to estimate λ_0 from the diffuse component when the Rq is known. Thus, the feasibility of surface topography characterization through the use of diffuse component of scattered air-coupled ultrasound has been demonstrated.

Acknowledgments

The financial supports from Grant-in-Aid for Scientific Researches (B17360351) by JSPS and the 21st Century Centers of Excellence (COE) Program of the Ministry of Education, Culture, Sports, Science and Technology are appreciated.

1) N. Tayebi and A. A. Polycarpou: Tribology Int. **37** (2004) 491.
2) S. Bjorklund: Tribology Int. **34** (2001) 841.
3) Y. Zhang and S. Sundararajan: J. Appl. Phys. **97** (2005) 103526.
4) D. J. Whitehouse: Meas. Sci. Technol. **8** (1997) 955.
5) J. M. Bennet: Meas. Sci. Technol. **3** (1992) 1119.
6) S. Yokozeki and T. Suzuki: Jpn. J. Appl. Phys. **9** (1970) 585.
7) X. M. Tong, H. Yamaoka, T. Uruga and E. Arakawa: Jpn. J. Appl. Phys. **32** (1993) L502.
8) K. Nagata, T. Umehara and J. Nishiwaki: Jpn. J. Appl. Phys. **12** (1973) 1693.
9) K. Mitsui: Precis. Eng. **8** (1986) 212.
10) D. D. Sukmana and I. Ihara: Jpn. J. Appl. Phys. **44** (2005) 4417.
11) J. A. Ogilvy: *Theory of Wave Scattering from Random Rough Surfaces* (IOP Publishing, Bristol, 1991).
12) Y. C. Shin, S. J. Oh and S. A. Cokker: J. Eng. Ind. **117** (1995) 439.
13) G. V. Blessing, J. A. Slowinski, D. G. Eitzen and H. M. Ryan: Appl. Opt. **32** (1993) 3433.
14) S. J. Oh, Y. C. Shin and E. S. Furgason: IEEE Trans. Ultrason. Ferroelectr. Freq. Control **41** (1994) 863.
15) M. deBilly, F. C. Tenoudji, G. Quentin, K. Lewis and L. Adler: J. Nondestr. Eval. **1** (1980) 249.
16) P. C. Pedersen and A. Grebe: Ultrasonics **39** (2001) 101.
17) J. E. Wilhjelm, P. C. Pedersen and S. M. Jacobsen: IEEE Trans. Ultrason. Ferroelectr. Freq. Control **48** (2001) 511.
18) M. de Billy, F. C. Tenoudji, A. Jungman and G. J. Quentin: IEEE Trans. Ultrason. Ferroelectr. Freq. Control **23** (1976) 356.
19) P. F. Smith and M. A. Player: Meas. Sci. Technol. **2** (1991) 419.
20) H. Nagahara, T. Hashida, M. Suzuki and M. Hashimoto: Jpn. J. Appl. Phys. **44** (2005) 4485.
21) D. W. Schindel, D. A. Hutchins, L. Zou and M. Sayer: IEEE Trans. Ultrason. Ferroelectr. Freq. Control **42** (1995) 42.
22) K. Tsubaki, H. Yamanaka, K. Kitada, T. Komoda and N. Koshida: Jpn. J. Appl. Phys. **44** (2005) 4436.
23) K. Sasaki, M. Nishihara and K. Imano: Jpn. J. Appl. Phys. **44** (2005) 4411.
24) K. Sasaki, M. Nishihara and K. Imano: Jpn. J. Appl. Phys. **43** (2004) 3071.
25) R. Stoessel, N. Krohn, K. Pfleiderer and G. Busse: Ultrasonics **40**

(2002) 159.
26) D. W. Schindel and D. A. Hutchins: IEEE Trans. Ultrason. Ferroelectr. Freq. Control **42** (1995) 51.
27) Ref. 11, Chap. 4, pp. 88–89.
28) Ref. 11, Chap. 1, p. 5.
29) D. H. Berman and J. S. Perkins: J. Acoust. Soc. Am. **78** (1985) 1045.
30) D. K. Dacol: J. Acoust. Soc. Am. **88** (1990) 978.
31) A. Sentenac, G. Toso and M. Saillard: J. Opt. Soc. Am. A **15** (1998) 924.
32) M. L. Boyd and R. L. Deavenport: J. Acoust. Soc. Am. **53** (1973) 791.
33) E. I. Thorsos: J. Acoust. Soc. Am. **83** (1988) 78.
34) O. Bozma and R. Kuc: J. Acoust. Soc. Am. **89** (1991) 2519.
35) F. T. Ulaby, R. K. Moore and A. K. Fung: *Microwave Remote Sensing: Active and Passive* (Addison-Wesley, Reading, MA, 1982) Vol. 2, Chap. 11.